Additively Manufactured Ceramics for High-Temperature Heat Rejection Systems

Giancarlo D'Orazio and Sadaf Sobhani

Cornell University

ABSTRACT

Plans to send crewed space flights beyond the Earth's sphere of influence require significant advances in spacecraft propulsion systems and electricity generation. Nuclear electric propulsion (NEP) offers higher specific impulse than conventional chemical rockets at the cost of extreme thermal loads. Heat rejection for NEP systems requires a careful balance of high temperature resistance and high thermal conductivity to dissipate energy from the source to the radiators. The current state of the art for high thermal conductivity heat rejection relies on titanium-ammonia heat pipes which are ineffective at temperatures exceeding 500 K. This study investigates the use of additively manufactured ceramics, specifically aluminum nitride (AlN), as a heat pipe material for high temperature applications beyond 500 K. AlN is chosen for its ability to operate within a wide temperature range, low system mass, excellent bulk thermal conductivity, and minimal chemical reactivity. Additive manufacturing enables the printing of the heat pipe structure, wick, and radiator panel in a single piece and without additional machining, thus reducing losses in the heat transfer system while reducing part complexity.

In this work, AlN has been developed for additive manufacturing via digital light processing wherein ceramic particles are dispersed into a photosensitive resin to form a slurry. The AlN slurry has been evaluated for depth of cure, interlayer adhesion, and viscosity. Initial experiments show good compatibility with the Admatec Admaflex 130 digital light processing printer. Prospective wick designs have been printed in alumina (Al_2O_3) for initial testing at atmospheric conditions with acetone to determine the permeability and effective capillary meniscus radius. AlN test articles have been printed to examine flexural strength, thermal conductivity, and working fluid chemical compatibility in addition to thermal characteristics such as bulk thermal conductivity and emissivity.

NOMENCLATURE

C	=	Characteristic length (e.g. wavelength, m)
D_{cure}	=	Depth of cure (μm)

d_{part} = Mean particle diameter (μm)
E_{dose} = Dose energy density ($\frac{mJ}{cm^2}$)
g = Gravity ($\frac{m}{s^2}$)
h = Rise height (m)
I = Light intensity ($\frac{mW}{cm^2}$)
I_0 = Light intensity to cure resin ($\frac{mW}{cm^2}$)
K = Permeability (m^2)
P_c = Capillary pressure (Pa)
r_{eff} = Effective capillary meniscus radius (m)
t = Time (s)
Δ_n = Difference between refractive index of n_0 and ceramic
ε = Porosity
ϕ = Volumetric particle loading
ρ = Density ($\frac{kg}{m^3}$)
σ = Surface tension (N/m)

INTRODUCTION

Nuclear electric propulsion (NEP) has been proposed for long-distance crewed space flight missions, as life-support, propulsion, and science requirements impose a substantial demand [1]. While proposed nuclear reactors for space flight are capable of producing power in the megawatt range, these systems also produce considerable waste heat, with reactor outlet temperatures of up to of 1,500 K [2]. In order to accommodate a 2 MW_e NEP system, Machemer et al. propose a radiator area of approximately 4030 m^2 for a proposed water-based heat pipe cooling system, typical many spacecraft heat rejection designs [3]. While these systems have been proven robust, they are limited in two primary areas. First, metal-based heat pipes encounter significant working fluid incompatibilities due to corrosion or reactivity. This precludes a number of potential fluids which can operate at temperatures higher than water and ammonia regimes. Secondly, many of the lightweight metals best suited to spacecraft thermal transfer systems have relatively low melting points, exposing the system potential failures due to creep and thermal fatigue with extended use at high temperatures. This work considers the use of additively manufactured ceramic heat pipe and radiator components as a means to overcome these issues. The low density of certain ceramics, paired with high temperature stability and low reactivity provide a path forward for heat rejection systems which can operate at higher temperature than the effective limits attainable with metal-water/ammonia systems [4, 5]. Such a system would integrate a heat pipe and radiator panel as a single, monolithic part, and transfer waste heat from the reactor's pumped fluid loop to the heat pipe, as seen in Figure 1. The ultimate design of this system is intended to include an approximately 1 m^2 radiator panel with integrated 20 internal diameter cm heat pipe, the specifics of which are to be finalized after significant testing of the AlN printing process and working fluid compatibility tests.

Additive manufacturing presents unique opportunities to develop intricate monolithic heat pipe and radiator panel systems, obviating a number of fabrication steps, integrating parts, and enabling arbitrarily complex wick structures. In this space, much recent work

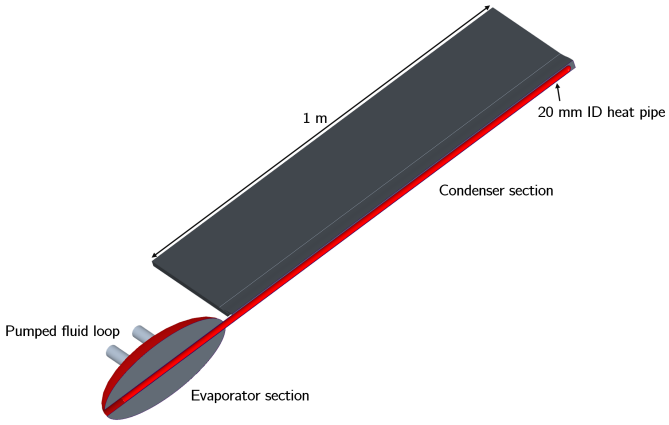

Figure 1: Simplified section view diagram illustrating the radiator and heat pipe assembly with the reactor pumped fluid loop.

has been done examining metal AM, particularly utilizing selective laser melting [6–12]. In comparison, ceramic AM is a comparatively new technology, and its use as heat pipe material has considerable room for exploration. Conventional ceramics have been proposed for use in heat pipes, for instance Hack et al. demonstrated a novel silicon carbide ceramic pipe with zinc working fluid [13]. This design did not utilize a wick structure, instead relying on wetting the solid pipe walls. Work by Sixel, et al. considered AM alumina heat pipes for use in electric motors, where the high dielectric strength of the ceramic and high temperature tolerance are an excellent match [14, 15]. Importantly, they demonstrated and integrated wick structure using sintered spherical alumina powder. While alumina is a stable material and comparatively easy to print and process [16], it has poor heat transfer and thermal shock characteristics compared to aluminum nitride (AlN).

Aluminum nitride has excellent thermal properties with high thermal conductivity (>120 W/m·K), low bulk density, and high thermal shock resistance. It does, however, present some issues with light-based printing processes such as digital light processing, owing to its high refractive index which limits the depth of cure of photosensitive resin binder. Equation 1 is an approximation for depth of cure based a number of parameters based on the resin and the ceramic particles:

$$D_{cure} \approx \frac{C}{\phi} \cdot d_{part} \left(\frac{n_0}{\Delta_n} \right)^2 \cdot ln \left(\frac{I}{I_0} \right) \tag{1}$$

In this equation, D_{cure} is the depth of cure in μm, C is a characteristic length, frequently the light exposure wavelength, ϕ is the volumetric particle loading, d_{part} is the mean particle diameter, n_0 is the refractive index of the base resin, Δ_n is the difference in refractive index between the resin and ceramic particles, I is the curing intensity required to achieve a target D_{cure}, and I_0 is the light intensity to cure the base resin. Increasing particle size will improve depth of cure, however these larger grains produce weaker ceramics with worse thermal characteristics in general. Volumetric particle loading is maintained at a constant 40%, itself a compromise between depth of cure and slurry viscosity. The refractive index of the AlN powder is approximately 2.109 at 405 nm [17], a considerable difference between that of the resin at approximately 1.46. Materials such as silica and alumina have lower refractive

Table 1. Comparison of AM AlN Compositions

	Composition (wt %)	Sintering Temperature (°C)	Flexural Strength (MPa)	Thermal Conductivity (W/m·K)
Duan et al. 2020 [21]	95:5 $AlN:Y_2O_3$	1845	265 ± 20	155
Ożóg et al. 2020 [25]	90:6:4 $AlN:Y_2O_3:Al_2O_3$	1800	Not tested	4.34
Lin et al. 2022 [22]	100:5 $AlN:Y_2O_3$	1850	365-400	135-150 (appr)
Rauchenecker et al. 2022 [23]	96:3:1 $AlN:Y_2O_3:CaO$	1700	320-498	162.1-166.2
Lee and Kim 2014 [24] (Basis for this work, non AM)	98:1:1 $AlN:Y_2O_3:CaZrO_3$	1600	579	120

indices, 1.470 and 1.786 at 405 nm respectively [18, 19] and thus require between 6-10 times lower light intensity to receive the same depth of cure.

To date, a number of groups have successfully printed AlN ceramics with conventional formulations leveraging yttria (Y_2O_3) or a blend of yttria and alumina as a liquid-state sintering aids [20–22]. In all cases, sintering temperatures exceeded 1780°C. These high temperatures are limiting in terms of processing, as there are comparatively few commercial sintering furnaces which can process at such temperatures. Work by Rauchenecker et al. utilized calcium oxide (CaO) in addition to yttria as a sintering aid to enable liquid-state sintering at temperatures as low as 1700°C while maintaining high thermal conductivity, greater than 160 W/m·K [23]. This work examines the novel low-temperature sintering formulation proposed by Lee and Kim which adds calcium zirconate ($CaZrO_3$) to the conventional yttria sintering aid to produce a high-strength final product with high thermal conductivity [24]. Additionally, processing temperatures are significantly lower than in other works, as low as 1500°C in some formulations. A summary of these formulations and their material properties are presented in Table 1.

Work by Sarraf and Anderson isolated several promising working fluids in their analysis of a variety of envelope materials and working fluids in the 400-800K operating regime [26]. Owing primarily to handling issues, prospective materials such as cesium were not considered, in preference for stable, minimally hazardous substances. In particular, Dowtherm A was considered, as a comparatively safe and well characterized working fluid. Additionally, halides, particularly aluminum bromide ($AlBr_3$), aluminum chloride ($AlCl_3$), iodine (I_2), and iron chloride ($FeCl_3$) were selected for study. These working fluids have significant corrosion potential with different metal heat pipes, however study is undergoing to determine their interactions with comparatively inert aluminum nitride.

EXPERIMENTAL DESIGN

An Admatec Admaflex 130 digital light processing 3D printer was used to test and print AlN samples. This system relies on 405 nm near-UV light to cure a photosensitive resin binder with ceramic particles in suspension. The printer builds in layers between 10 and 50 μm in

thickness, forming a solid green body ceramic which is subsequently thermally processed, or debound, to burn off the resin. The remaining ceramic particles are sintered to final density without impurities from the binder. Hogänäs Grade C aluminum nitride was selected as the base ceramic, owing to its particle size distribution between 800 and 2000 nm; this strikes a balance between high strength due to small particle size and allowing adequate depth of cure based on light mean free path.

The sintering aids calcium zirconate ($CaZrO_3$, 40 nm, SigmaAldrich) and yttria (Y_2O_3, 10 nm, US Research Nanomaterials) were added 1%/weight each to the AlN base powder. Hypermer KD1 dispersant was then added in a ratio of 1%/weight to the resultant mixture. Acetone sufficient to wet the powder blend was added and was mixed in a Speedmixer Flaktek 1200-700 VAC mixer at 1,000 RPM for 2 minutes. The acetone was subsequently evaporated at 35°C for 24 hours and the resultant powder-dispersant mix ground with a mortar and pestle and sieved to 53 μm. This fine powder was vacuum desiccated for a period of 24 hours and added to Admatec Development Resin C (Admatec) in a 40%/volume ratio and mixed with the Flacktek mixer from 800 to 1,200 RPM in 30 second, 100 RPM increments.

The ceramic-resin slurry was stored for 24 hours before rheometry and depth of cure testing to ensure proper ceramic suspension. The viscosity was characterized with a TA Instruments DHR3 Rheometer from a shear rate (1/s) of 0.01 to 100. Small quantities of the slurry were exposed between 70 and 85% of the maximum LED power of the Admaflex 130 printer for durations of 10-20 seconds to determine depth of cure. Small printed samples were process for thermogravimetric analysis (TGA) with a TA Instruments TGA5500 in air and nitrogen with a heating rate of 2°C per minute to develop a debinding curve for printed parts.

Prospective wick designs were created using PTC Creo Parametric and nTopology. Designs with pore sizes of less than 300 μm were developed and subsequently printed in alumina as flat wicks for rate of rise testing. Alumina was chosen due to the ease of processing, relying on only air atmosphere ovens, and faster printing speed. Wicks were suspended by a magnet in a test tube acetone, as illustrated in Figure 2. Samples were slowly lowered to the point that they touched the acetone and resultant working fluid flow behavior captured on a camera, whereupon the rate of rise and total rise height measured, the testing and analysis of which are ongoing. From these experiments, the capillary pressure, P_c, can be estimated in steady state as a function of density, d, gravity, g, and rise height, h, as in Equation 2. Additionally, measurement of rise over time, $\frac{dh}{dt}$, yields the wick permeability, K, and effective capillary radius, r_{eff}, provided the porosity of the wick, ε, and the dynamic viscosity, μ, and surface tension, σ, of the working fluid, as shown in Equation 3. The testing of these wick structures is currently ongoing.

$$P_c = \rho g h \tag{2}$$

$$h\frac{dh}{dt} = \frac{K}{\varepsilon\mu}\left(\frac{2\sigma}{r_{eff}} - \rho g h\right) \tag{3}$$

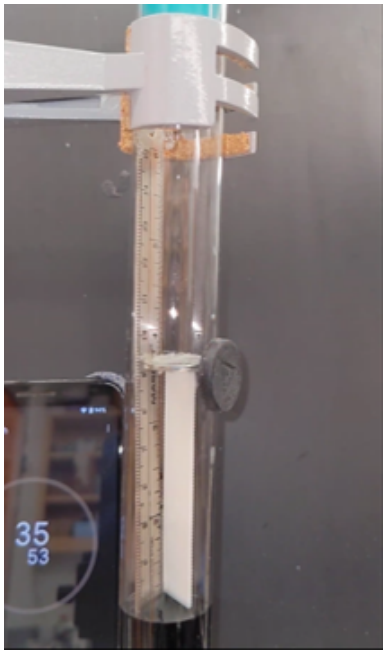

Figure 2: Sample alumina wick with diamond triply periodic minimal surface lattice in rate of rise test apparatus.

RESULTS

The prepared AlN slurry proved adeqaute for use in the Admaflex 130 printer, with viscosity suitable for the recirculation and build plate systems. The results of the rheometry in Figure 3 shows that the slurry exhibits shear thinning behavior below a shear rate of 32 1/s. This ensures compatibility with the printing system, notably the peristaltic slurry recirculating pump, doctor knife to apply appropriate slurry thickness, and build head settling time as it presses into the slurry layer.

The slurry was subsequently tested for depth of cure with an Admatec Admaflex 130 digital light processing 3D printer over a range of exposure powers and duration. Effective energy dose is estimated in Equation 4:

$$E_{dose} \approx 46\ mW/cm^2 * LED\% * t \tag{4}$$

Where the dose energy density in mJ/cm^2, E$_{dose}$, is a function of the percentage of maximum LED power times the exposure time, t, in seconds. Testing with the Admatec printer resulted in a maximum depth of cure of 34 μm with an LED power of 75% of maximum for 12 seconds, a dose of approximately 414 mJ/cm^2. Owing to this maximum depth of cure, a 20 μm layer height was selected, optimizing print speed with respect to cure depth. Interlayer adhesion tested by printing ASTM C1161-B bending beams; these beams are to be debound and tested in a four point bending test apparatus to ascertain flexural strength.

Thermogravimetric analysis was conducted in air and nitrogen atmospheres to compare the derivative mass loss and loss percent of the samples. TGA of test samples in air, the results of which are shown in Figure 4, indicates three mass loss rate peaks based on the derivative of mass loss, at approximately 200, 350, and 455 °C. Some work has demonstrated

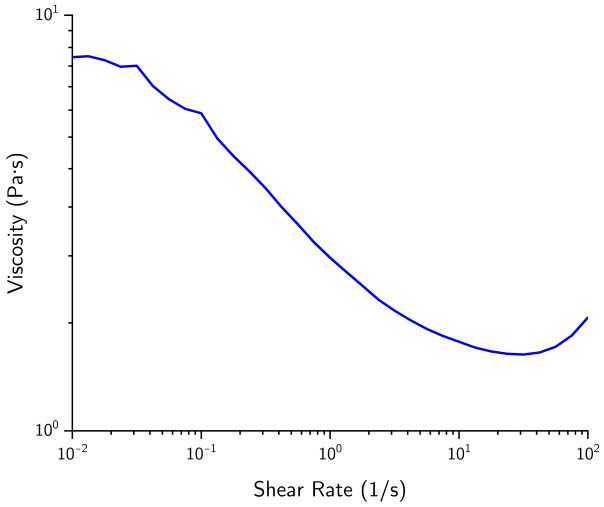

Figure 3: Shear thinning behavior of the as-prepared aluminum nitride slurry.

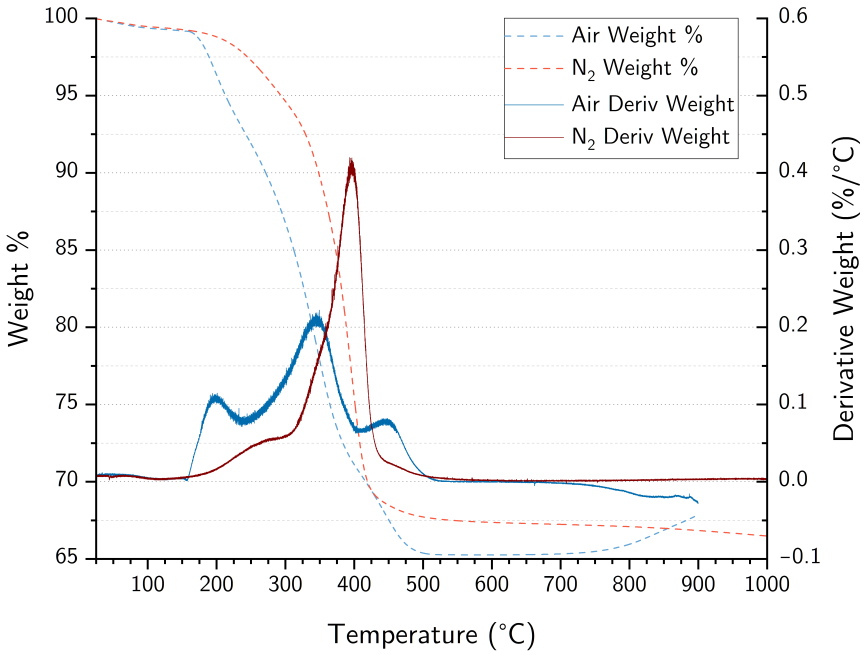

Figure 4: Thermogravimetric analysis of the green body, showing mass loss rate and derivative mass loss in both air and nitrogen atmospheres.

that AlN begins to oxidize at temperatures as low as 550°C as oxynitrides form, eventually converting to oxides above 900°C [27, 28]. This becomes apparent in the TGA beginning at 500°C as the mass loss begins to level then eventually gain mass beyond 700°C as AlN is gradually converted to more dense Al_2O_3. The TGA conducted nitrogen environment, by comparison, consists of a singular peak at approximately 400°C and no subsequent mass gain. The air debinding curve derived from this analysis is presented in Table 2 and was subsequently used when debinding test articles before sintering, however a nitrogen debinding process is in active development.

Table 2. AlN Debinding Curve in Air

Step	T1 (°C)	T2 (°C)	Rate/Time
1	20	150	65°C/hr
2	150	200	12°C/hr
3	200	200	2 hr
4	200	350	12°C/hr
5	350	350	2hr
6	350	400	12°C/hr
7	400	20	25°C/hr
		Total	42.03 hr

Air debound parts were sintered in a nitrogen atmosphere, heating from ambient to 1600°C at rate of 10°C per minute with a 3 hour hold, then cooling at a rate of 25°C per hour to 1400°C and held again for 2 hours. After this two-step sintering process, the parts were cooled at 25°C per hour. The sintered test beams, in Figure 5 demonstrate the that the lower temperature sintering process produces dense parts with approximately 12% shrinkage. Due to unwanted ambient oxygen, some oxidation occurred, producing a hybrid alumina-aluminum nitride ceramics. Process improvements are ongoing to better produce AlN parts, including increasing nitrogen flow rate to 2 standard liters per minute, and pressurizing the furnace to 14 kPa above ambient.

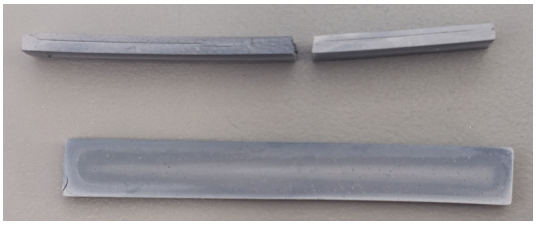

Figure 5: Sintered aluminum nitride beams, showing some oxidation and delamination.

A small-scale heat pipe section was printed which consisted of a rectangular outer shell 75 mm x 10 mm x 10 mm with a cylindrical internal wick structure 1 mm thick composed of a gyroid triply periodic minimal surface lattice with 300 μm thick walls. Loss of feature definition was due to overexposure, resulting in limited pore space within the structure as illustrated in Figure 6. A slice of the internal structure, as would be exposed to the AlN slurry, is also shown, highlighting the fine porous structure internal to the pipe. Modified

print settings, which balance LED power and exposure time with depth of cure produced high definition articles, as shown in Figure 7. This 20 mm diameter heat pipe section is representative of the intended quality for full-scale prints and the settings will be used for subsequent prints.

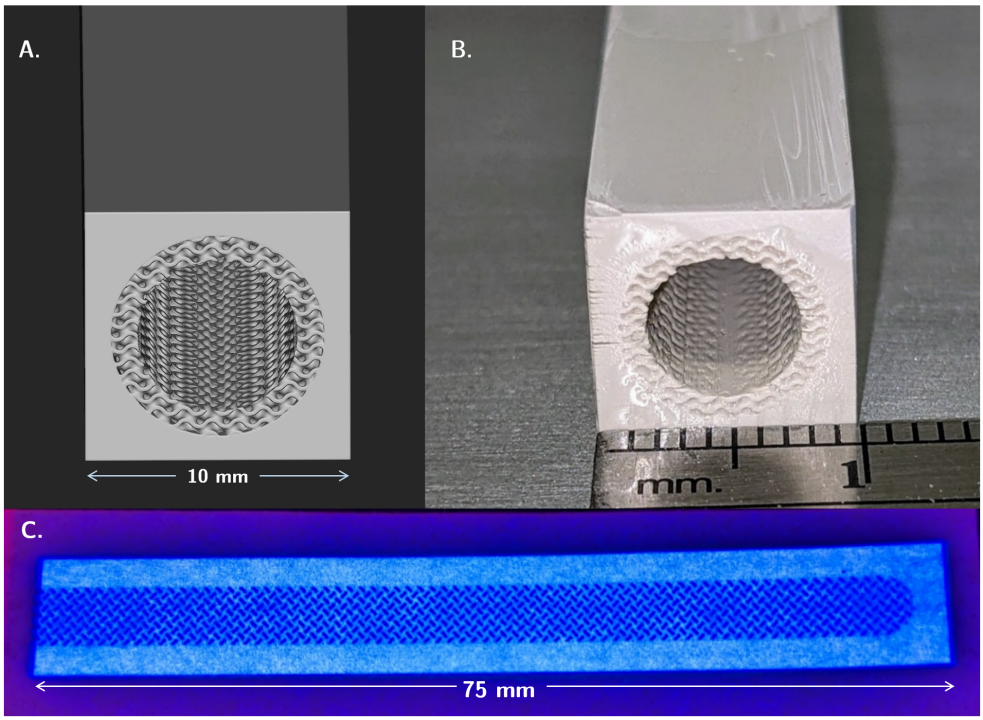

Figure 6: A. CAD model in nTopology of a sample heat pipe section. B. Sample heat pipe printed in aluminum nitride with gyroid lattice wick. C. a section cut of from the projector view illustrating the internal wick structure and supporting tube.

FUTURE WORK

Wick rate of rise testing is currently ongoing to better characterize the effective capillary radius and permeability of the prospective designs. Additional work is being conducted to better optimize the printer settings to reduce this overexposure while maintaining adequate depth of cure, balancing between exposure time and LED power. In typical operation, a light dose appropriate to cure to a depth of approximately twice that of the layer height is selected, however, subsequent parts will use lower exposure levels to prevent loss of fine features. In parallel, wick designs are also being explored may be less sensitive to overcuring. The printing process presented is constrained primarily by print volume thus restricting its use to small parts, however a high TRL panel design will considerably exceed the build volume of the current Admaflex 130 printer, as seen in Figure 1. DLP printing is highly scalable given that the technology is constrained only by projector area and Z-height. An obvious upgrade path then would be to utilize Admatec Admaflex 300 DLP printer, which

Figure 7: Optimized print settings, balancing print quality, interlayer adhesion, and print time produce high quality parts with fine feature definition.

has a 260 x 220 x 520 mm build volume, a nearly 52 times increase in volume over the Admaflex 130 used in this work.

CONCLUSIONS

The printing of a low sintering temperature formulation aluminum nitride was demonstrated with good interlayer adhesion and feature resolution at a 20 μm layer height. Thermogravimentric analysis was presented to facilitate the creation of a debinding curve in both air and nitrogen, however the propensity for aluminum nitride to begin to oxidize at temperatures above 400 °C indicates that nitrogen debinding produces a more desirable outcome without mass gain due to oxidation. Parts were then sintered in a two-step process with holds at 1600°C and 1400°C to produce dense, solid aluminum nitride ceramic. Additionally, a case for a scalable printing design is presented, with the capability to form integrated a radiator and heat pipe panel in a single print. This greatly increases throughput of the panels and consolidates a great number of parts in existing thermal management designs.

ACKNOWLEDGMENTS

The authors would like to thank William Sixel, Zachariah Chazen, Elaine Petro, and Andrew van Paridon for their support with this work.

The authors acknowledge the use of facilities and instrumentation supported by NSF through the Cornell University Materials Research Science and Engineering Center DMR-1719875.

REFERENCES

[1] V. P. Friedensen, "Space nuclear power: Technology, policy, and risk considerations in human missions to Mars," *Acta Astronautica*, vol. 42, no. 1, pp. 395–409, Jan. 1998. [Online]. Available: https://www.sciencedirect.com/science/article/pii/S0094576598001349

[2] A. S. Koroteev, Y. A. Oshev, S. A. Popov, A. V. Karevsky, A. Y. Solodukhin, L. E. Zakharenkov, and A. V. Semenkin, "Nuclear power propulsion system for spacecraft," *Thermal Engineering*, vol. 62, no. 13, pp. 971–980, Dec. 2015. [Online]. Available: https://doi.org/10.1134/S0040601515130078

[3] W. S. Machemer, M. E. Duchek, and D. Nikitaev, "Considerations for Radiator Design in Multi-Megawatt Nuclear Electric Propulsion Applications," in *AIAA SCITECH 2023 Forum*, ser. AIAA SciTech Forum. American Institute of Aeronautics and Astronautics, Jan. 2023. [Online]. Available: https://arc.aiaa.org/doi/10.2514/6.2023-0152

[4] T. C. Werner, Y. Yan, D. Mullen, and E. Halimic, "Experimental analysis of a high temperature water heat pipe for thermal storage applications," *Thermal Science and Engineering Progress*, vol. 19, p. 100564, Oct. 2020. [Online]. Available: https://www.sciencedirect.com/science/article/pii/S2451904920300822

[5] A. L. S. Sudhan, A. B. Solomon, and S. Sunder, "Heat transport limitations and performance enhancement of anodized grooved heat pipes charged with ammonia under gravity and anti-gravity condition," *Applied Thermal Engineering*, vol. 200, p. 117633, Jan. 2022. [Online]. Available: https://www.sciencedirect.com/science/article/pii/S1359431121010607

[6] O. T. Ibrahim, J. G. Monroe, S. M. Thompson, N. Shamsaei, H. Bilheux, A. Elwany, and L. Bian, "An investigation of a multi-layered oscillating heat pipe additively manufactured from Ti-6Al-4V powder," *International Journal of Heat and Mass Transfer*, vol. 108, pp. 1036–1047, May 2017. [Online]. Available: https://www.sciencedirect.com/science/article/pii/S0017931016331696

[7] D. Jafari, W. W. Wits, and B. J. Geurts, "Metal 3D-printed wick structures for heat pipe application: Capillary performance analysis," *Applied Thermal Engineering*, vol. 143, pp. 403–414, Oct. 2018. [Online]. Available: https://www.sciencedirect.com/science/article/pii/S1359431118322981

[8] R. J. MGlen, "An introduction to additive manufactured heat pipe technology and advanced thermal management products," *Thermal Science and Engineering Progress*, vol. 25, p. 100941, Oct. 2021. [Online]. Available: https://www.sciencedirect.com/science/article/pii/S2451904921001037

[9] A. J. Robinson, J. Colenbrander, T. Deaville, J. Durfee, and R. Kempers, "A wicked heat pipe fabricated using metal additive manufacturing," *International Journal of Thermofluids*, vol. 12, p. 100117, Nov. 2021. [Online]. Available: https://www.sciencedirect.com/science/article/pii/S2666202721000550

[10] D. Jafari and W. W. Wits, "Improving the performance of flat heat pipes by exploiting benefits of additive manufacturing," in *2022 28th International Workshop on Thermal Investigations of ICs and Systems (THERMINIC)*, Sep. 2022, pp. 1–6, iSSN: 2474-1523.

[11] S. Li, K. Essa, J. Carr, S. Chiwanga, A. Norton, and M. M. Attallah, "The development of a high-performance Ni-superalloy additively manufactured heat pipe," *Advances in Manufacturing*, vol. 10, no. 4, pp. 610–624, Dec. 2022. [Online]. Available: https://doi.org/10.1007/s40436-022-00407-z

[12] K.-L. Chen, K.-Y. Luo, P. P. Gupta, and S.-W. Kang, "SLM Additive Manufacturing of Oscillating Heat Pipe," *Sustainability*, vol. 15, no. 9, p. 7538, Jan. 2023, number: 9 Publisher: Multidisciplinary Digital Publishing Institute. [Online]. Available: https://www.mdpi.com/2071-1050/15/9/7538

[13] N. Hack, S. Unz, and M. Beckmann, "Ceramic Heat Pipes for High Temperature Application," *Energy Procedia*, vol. 120, pp. 140–148, Aug. 2017. [Online]. Available: https://www.sciencedirect.com/science/article/pii/S1876610217327133

[14] W. Sixel, M. Liu, G. Nellis, and B. Sarlioglu, "Ceramic 3D Printed Direct Winding Heat Exchangers for Improving Electric Machine Thermal Management," in *2019 IEEE Energy Conversion Congress and Exposition (ECCE)*, Sep. 2019, pp. 769–776, iSSN: 2329-3748.

[15] W. Sixel, M. Liu, G. Nellis, and B. Sarlioglu, "Ceramic 3-D Printed Direct Winding Heat Exchangers for Thermal Management of Concentrated Winding Electric Machines," *IEEE Transactions on Industry Applications*, vol. 57, no. 6, pp. 5829–5840, Nov. 2021, conference Name: IEEE Transactions on Industry Applications.

[16] M. Schwentenwein and J. Homa, "Additive Manufacturing of Dense Alumina Ceramics," *International Journal of Applied Ceramic Technology*, vol. 12, no. 1, pp. 1–7, 2015, _eprint: https://onlinelibrary.wiley.com/doi/pdf/10.1111/ijac.12319. [Online]. Available: https://onlinelibrary.wiley.com/doi/abs/10.1111/ijac.12319

[17] L. Y. Beliaev, E. Shkondin, A. V. Lavrinenko, and O. Takayama, "Thickness-dependent optical properties of aluminum nitride films for mid-infrared wavelengths," *Journal of Vacuum Science & Technology A*, vol. 39, no. 4, p. 043408, May 2021. [Online]. Available: https://doi.org/10.1116/6.0000884

[18] I. H. Malitson, F. V. Murphy, and W. S. Rodney, "Refractive Index of Synthetic Sapphire," *JOSA*, vol. 48, no. 1, pp. 72–73, Jan. 1958, publisher: Optica Publishing Group. [Online]. Available: https://opg.optica.org/josa/abstract.cfm?uri=josa-48-1-72

[19] I. H. Malitson, "Interspecimen Comparison of the Refractive Index of Fused Silica*,†," *JOSA*, vol. 55, no. 10, pp. 1205–1209, Oct. 1965, publisher: Optica Publishing Group. [Online]. Available: https://opg.optica.org/josa/abstract.cfm?uri=josa-55-10-1205

[20] P. Ożóg, P. Rutkowski, D. Kata, and T. Graule, "Ultraviolet lithography-based ceramic manufacturing (uv-lcm) of the aluminum nitride (aln)-based photocurable dispersions,"

Materials, vol. 13, no. 19, 2020. [Online]. Available: https://www.mdpi.com/1996-1944/13/19/4219

[21] W. Duan, S. Li, G. Wang, R. Dou, L. Wang, Y. Zhang, H. Li, and H. Tan, "Thermal conductivities and mechanical properties of AlN ceramics fabricated by three dimensional printing," *Journal of the European Ceramic Society*, vol. 40, no. 10, pp. 3535–3540, Aug. 2020. [Online]. Available: https://www.sciencedirect.com/science/article/pii/S0955221920302594

[22] L. Lin, H. Wu, P. Ni, Y. Chen, Z. Huang, Y. Li, K. Lin, P. Sheng, and S. Wu, "Additive manufacturing of complex-shaped and high-performance aluminum nitride-based components for thermal management," *Additive Manufacturing*, vol. 52, p. 102671, Apr. 2022. [Online]. Available: https://www.sciencedirect.com/science/article/pii/S2214860422000768

[23] J. Rauchenecker, J. Rabitsch, M. Schwentenwein, and T. Konegger, "Additive manufacturing of aluminum nitride ceramics with high thermal conductivity via digital light processing," *Open Ceramics*, vol. 9, p. 100215, Mar. 2022. [Online]. Available: https://www.sciencedirect.com/science/article/pii/S2666539521001619

[24] H. M. Lee and D. K. Kim, "High-strength AlN ceramics by low-temperature sintering with CaZrO3–Y2O3 co-additives," *Journal of the European Ceramic Society*, vol. 34, no. 15, pp. 3627–3633, Dec. 2014. [Online]. Available: https://www.sciencedirect.com/science/article/pii/S0955221914002660

[25] S. Ozguc, S. Pai, L. Pan, P. J. Geoghegan, and J. A. Weibel, "Experimental Demonstration of an Additively Manufactured Vapor Chamber Heat Spreader," in *2019 18th IEEE Intersociety Conference on Thermal and Thermomechanical Phenomena in Electronic Systems (ITherm)*, May 2019, pp. 416–422, iSSN: 2577-0799.

[26] D. B. Sarraf and W. G. Anderson, "Heat Pipes for High Temperature Thermal Management." American Society of Mechanical Engineers Digital Collection, Jan. 2010, pp. 707–714. [Online]. Available: https://asmedigitalcollection.asme.org/InterPACK/proceedings-abstract/InterPACK2007/42770/707/324319

[27] A. D. Katnani and K. I. Papathomas, "Kinetics and initial stages of oxidation of aluminum nitride: Thermogravimetric analysis and x-ray photoelectron spectroscopy study," *Journal of Vacuum Science & Technology A*, vol. 5, no. 4, pp. 1335–1340, Jul. 1987. [Online]. Available: https://doi.org/10.1116/1.574765

[28] A. Bellosi, E. Landi, and A. Tampieri, "Oxidation behavior of aluminum nitride," *Journal of Materials Research*, vol. 8, no. 3, pp. 565–572, Mar. 1993. [Online]. Available: https://doi.org/10.1557/JMR.1993.0565